Composites Part B 94 (2016) 379–388

Contents lists available at ScienceDirect

Composites Part B

journal homepage: www.elsevier.com/locate/compositesb

Planar auxeticity from elliptic inclusions

Artur A. Poźniak [a], Krzysztof W. Wojciechowski [b, *], Joseph N. Grima [c, d], Luke Mizzi [d]

[a] Department of Technical Physics, Poznan University of Technology, Piotrowo 3, 60-965 Poznań, Poland
[b] Institute of Molecular Physics, Polish Academy of Sciences, M. Smoluchowskiego 17, 60-179 Poznań, Poland
[c] Department of Chemistry, Faculty of Science, University of Malta, Msida, MSD 2080, Malta
[d] Metamaterials Unit, Faculty of Science, University of Malta, Msida, MSD 2080, Malta

ARTICLE INFO

Article history:
Received 18 August 2015
Received in revised form
3 March 2016
Accepted 11 March 2016
Available online 2 April 2016

Keywords:
B. Mechanical properties
A. Smart materials
C. Finite element analysis (FEA)
Negative Poisson's ratio

ABSTRACT

Composites with elliptic inclusions of long semi-axis a and short semi-axis b are studied by the Finite Element method. The centres of ellipses form a square lattice of the unit lattice constant. The neighbouring ellipses are perpendicular to each other and their axes are parallel to the lattice axes. The influence of geometry and material characteristics on the effective mechanical properties of these anisotropic composites is investigated for deformations applied along lattice axes. It is found that for anisotropic inclusions of low Young's modulus, when $a + b \to 1$ the effective Poisson's ratio tends to -1, while the effective Young's modulus takes very low values. In this case the structure performs the rotating rigid body mechanism. In the limit of large values of Young's modulus of inclusions, both effective Poisson's ratio and effective Young's modulus saturate to values which do not depend on Poisson's ratio of inclusions but depend on geometry of the composite and the matrix Poisson's ratio. For highly anisotropic inclusions of very large Young's modulus, the effective Poisson's ratio of the composite can be negative for *nonauxetic* both matrix and inclusions. This is a very simple example of an auxetic structure being not only entirely continuous, but with very high Young's modulus. A severe qualitative change in the composite behaviour is observed as a/b reaches the limit of 1, i.e. inclusions are isotropic. The observed changes in both Poisson's ratio and Young's modulus are complex functions of parameters defining the composite. The latter allows one to tailor a material of practically arbitrary elastic parameters.

1. Introduction

The negative Poisson's ratio (NPR) materials [1,2] coined *auxetics* [3], have attracted an increasing interest during last three decades. There are several mechanisms leading to the auxetic behaviour of solids [1,4,5,3,7–10] One of them is the rotating rigid units mechanism which has been a subject of intensive studies [11–15]. As it is well known, that mechanism acts on various length-scales: from nano to macro scale [11–16] and can be relatively easy applied to engineering of materials with negative Poisson's ratio [17–19]. Namely, one can cut holes of certain shapes in various (periodic) manners in order to obtain rigid units connected with narrow regions imitating the hinges allowing the rigid units to rotate [17,18,20–24]. The elliptic voids were introduced for the first time in the paper by Bertoldi and co-workers [25]. (In fact, the elliptic shape of the initially circular inclusions was a consequence of buckling accompanying the uniaxial compression.) Once the periodic pattern of holes is cut, the voids can be filled with a material of different mechanical properties. This leads to the idea of periodic composites made of auxetic and/or conventional materials.

The concept of composites with auxetic inclusions was investigated in a series of publications by Wei and Edwards [26–29] who proposed approximate analytic solutions for three-dimensional random composites of auxetic inclusions in frames of the mean field theory. Recently, the notion of auxetic phase as a constituent of a composite was discussed by Assidi and Ganghoffer [30] and Strek and co-workers [31–34]. An interesting auxetic composite material which becomes even more auxetic during stretching was studied by Hou et al. [35]. Christensen [36] considered effective properties of a composite consisting of elastic matrix with rigid spherical inclusions. The latter work is worth to be mentioned here because one of the aims of the present paper is the analysis of the limit of rigid inclusions. Discussing composites containing anisotropic inclusions, one should not forget about the important role of orientation of inclusions, discussed e.g. in the work by Banks-Sills and co-workers [37].

In the present work, the attention is focused on effective mechanical properties of systems with elliptic inclusions of Young's modulus varying from 0 (void inclusions) to ∞ (perfectly rigid

* Corresponding author.
E-mail address: kww@man.poznan.pl (K.W. Wojciechowski).

http://dx.doi.org/10.1016/j.compositesb.2016.03.003
1359-8368/

inclusions). Axes of neighbouring ellipses of centres forming a square lattice (of axes x, y) are perpendicular to each other and parallel to x or y axis, respectively. The aim of this research is to establish the effective (macroscopic) mechanical properties of such a composite. The composite is not isotropic. However, for simplicity, this work is focused on mechanical properties along the x axis being the direction of applied force. (Studies of the general case will be the next step.) The analysis is performed by the finite element method, as it has already been successfully used in solving other composite structures [38,39]. We should add here that a preliminary stage of this research was discussed during the 8th Workshop on "Auxetics and Related Systems" on September 2011 in Szczecin, Poland [40].

The article is organized as follows. In the Section 2 the model is introduced, i.e. geometry of the composite and materials forming it are defined. In the Section 3 the method of solving the model is described. In the Section 4 the results are presented and discussed. Section 5 contains the summary and conclusions. Finally, in the Appendix A the convergence and accuracy of the numerical solutions are considered and the Appendix B contains results for a few geometries that were not included in the article body to avoid the legibility reduction.

2. The model

The subject of present studies are planar (2D) structures consisting of the matrix, wherein the elliptical inclusions are arranged in the periodic manner, see Fig. 1a. As shown in Fig. 1b, the centers of inclusions form the square lattice of the lattice constant $D = L_0/2$, where D is further taken as a unit on length and L_0 stands for the square-shaped periodicity box dimension. The elliptical inclusions have two possible orientations, horizontal and vertical, with nearest neighbours being always perpendicular to each other, see Fig. 1a. The unit cell of the analyzed structure is presented in Fig. 1b. The parameters A and B shown there are the only geometrical factors describing the semi-major and semi-minor axes of the ellipses respectively. In this paper dimensionless (divided by the lattice constant D) geometrical parameters $a = A/D$ and $b = B/D$ are also used.

The structure defined above can be seen as an analogue of either the rotating square model [11] with square-like elements of the matrix shown in Fig. 1c or as anti-tetrachiral arrangement of the latter elements [41,6,42]. It is convenient to define another (dependent) geometrical quantity $L_{\mathrm{gap}} = (1 - a - b)D$ describing the thickness of the narrowest region of the matrix which is the smallest distance between the neighbouring inclusions, see Fig. 1a. The mentioned narrow region will be further referred to as a *neck*. These necks act as hinges in the rotating square model or as ribs in the anti-tetrachirals.

Apart from the geometrical parameters of the structure, the mechanical properties of the composite constituents are of essential importance. Elastic properties of isotropic materials within the linear elasticity theory are fully characterized by only two quantities [43]. In this work Young's modulus, E, and Poisson's ratio, ν, play this role. In the presented system the following parameters are variable: Poisson's ratio of the matrix (ν_{matr}) and inclusions (ν_{incl}), as well as the Young's modulus of the inclusions (E_{incl}). These parameters are as follows:

$$\nu_{\mathrm{matr}} \in \{-0.99, -0.49, 0.0, 0.49\},$$

$$\nu_{\mathrm{incl}} \in \{-0.99, -0.49, 0.0, 0.49\},$$

$$E_{\mathrm{incl}} = 10^i (\text{in proper units}), \quad \text{where } i = -8, -7, \ldots, 6.$$

It is worth to add that the Young's modulus (E_{matr}) of the matrix plays the role of the reference value, being constant and equal to unity (in proper units). Possibility of such a choice of the matrix Young's modulus is a consequence of the linear elasticity used in this work. Since the solution of the equations is scalable, it is enough to control the ratio $E_{\mathrm{incl}}/E_{\mathrm{matr}}$. Using a linear transformation the obtained solution can be then scaled to a particular value of E_{matr}. In turn, the values of the Poisson's ratio for both materials have been selected in the way presented above to avoid singularities which occur (in the 3D elasticity) for $\nu \in \{-1, 1/2\}$, whereas $\nu = -0.49$ is the negative approximation of the upper bound of Poisson's ratio $(1/2)$ in 3D isotopic elasticity.

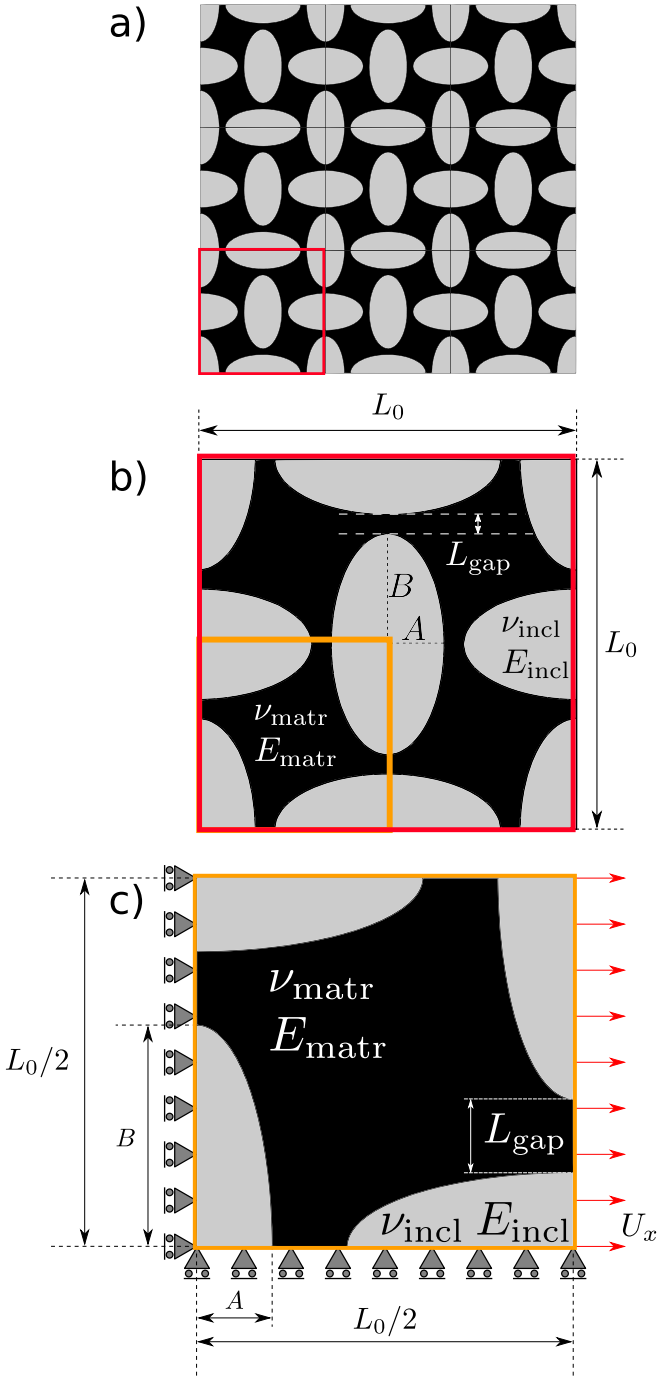

Fig. 1. Geometry of the structure (a), within a selected RUC (b) and simulated quarter with prescribed boundary conditions (c). All boundaries marked with orange lines in Fig. (c) remain straight lines and do not undergo rotations. (For interpretation of the references to colour in this figure legend, the reader is referred to the web version of this article.)

One should also stress that the materials of both matrix and inclusions are Hookean and isotropic. In consequence, the results for large strains (Fig. 9) presented in the final part of the paper take into account only the geometrical nonlinearities.

As mentioned earlier, the structure shown in Fig. 1 can be seen as an analogue of either the anti-tetrachiral structure (excluding the particular case $a = b$) [42] or the rotating square one [11]. Thus, in the limit $L_{gap}/D \to 0$, a negative Poisson's ratio equal to -1 (except when $a = b$) for the composite studied in the case $E_{incl}/E_{matr} \to 0$ (void inclusions) is just a consequence of the existence of the mentioned rotating rigid units mechanisms. This is because there are known analytical expressions for the mechanical properties in the idealized rotating units models. In the case of the present model, however, when non-empty elliptical inclusions with variable hardness are investigated, no exact solutions exist and numerical simulations have to be performed. In the following section the simulation method is discussed.

3. Method of solution

As the studied structures are perfectly periodic, i.e. without any disorder, the *repeating unit cell* (RUC) approach [44,45] can be used in simulations. The RUC, being the periodicity box, is illustrated in Fig. 1b. Using the RUC-based simulation instead of simulating large samples reduces computational costs due to small size of the simulation domain. However, thanks to the symmetry of the RUC, the computational region can be further reduced to its quarter, as shown in Fig. 1c. This reduction must be accompanied by introduction of certain constraints that are described later.

For a single set of parameters characterizing the non-deformed system, it is possible to evaluate ν_{eff} and E_{eff} within only one simulation step – an uniaxial stretching deformation with the mandatory use of constraints keeping the boundaries straight lines. The system remains constrained in such a way for symmetry reasons and in order to eliminate the rigid-body translations and rotations of the defined quarter of RUC. The roller symbols along the left and bottom boundaries indicate boundary conditions eliminating a single degree of freedom (x for the left symbol and y for the bottom one) keeping the boundaries straight, which is an immediate consequence of the RUC symmetry. In order to establish the values of elastic constants the structure undergoes an uni-axial stretching along the x direction by applying a displacement-type boundary condition. The displacement field applied to the right boundary denoted in Fig. 1c by red arrows reads $\{U_x, 0\}$ and remains constant along the boundary. The system is allowed do deform in the y direction keeping the upper boundary as a straight horizontal line. To evaluate the Poisson's ratio and the Young's modulus one should establish the *vertical displacement* of a node belonging to the upper boundary and the *elastic deformation energy*, respectively. Let L_x and L_y denote the width and the height of the RUC quarter, respectively. W stands for the elastic deformation energy while T denotes the plane stress thickness (U_x has already been introduced in Fig. 1c as the value of the applied displacement). The effective Young's modulus reads (see the equation 3 in page 5455 in the recent paper by Xie and Fan [46]):

$$E_{eff} = \frac{2\ W\ L_x}{T\ U_x^2\ L_y}. \tag{1}$$

As there is neither any reference nor a derivation of the equation (1) in the paper by Xie and Fan, we sketch a derivation here. One starts with the definition of the strain energy per unit volume, $W = 1/2\ \sigma_x\ \epsilon_x$ [47], where $\sigma_i = \epsilon_i\ E_{eff}$ denotes the stress, while $\epsilon_i = U_i/L_i$ stands for the macroscopic strain. Both values are supposed to occur during the uniaxial stretching. Multiplying this relation by the specimen dimensions in the reference state (L_x, L_y, T), substituting σ_x by the product $\epsilon_x\ E_{eff}$ and keeping in mind that $\epsilon_x = U_x/L_x$, one gets: $W = 1/2\ \epsilon_x\ E_{eff}\ \epsilon_x\ L_x\ L_y\ T = 1/2(U_x^2\ E_{eff}\ L_y\ T/L_x)$. Expressing E_{eff} through the other quantities in the latter equality, one immediately gets the equation (1). (To check the correctness of the equation (1), a series of extra tests was performed, in which mechanically uniform rectangular domain of selected values of E_{eff} and ν was stretched. The values of Young's moduli calculated by using (1) were equal to the selected ones with the accuracy of 6th decimal place.)

If the vertical component (y) of the displacement of arbitrary top node is denoted by U_y, then the effective Poisson's ratio for loading in the horizontal (x) direction reads:

$$\nu_{eff} = -\frac{U_y/L_y}{U_x/L_x}. \tag{2}$$

The above equation comes directly from the definition of Poisson's ratio in the xy-plane for loading in the x-direction: $\nu = -\epsilon_y/\epsilon_x$.

An important part of the finite element (FE) simulation is the proper discretization of the continuum. It has been observed that for small values of L_{gap} together with low Poisson's ratio $\nu_{matr} \to -1$ the simulated structures were prone to significant numerical error. The origin of this error was insufficient mesh quality. The latter, in general, means too low density of mesh, particularly in regions which undergo the largest deformations. One of such critical regions are the necks of the matrix. The neck's dimension is measured by the quantity L_{gap}. For instance, in Fig. 2 there are drawn eight layers of elements across the neck.

Using uniform mesh with all elements being roughly of the same size, would be, in principle, a simple and safe strategy for a large number of elements. However, this approach is very inefficient. Large number of elements requires huge computational resources. A smart distribution of element sizes along the edges should reduce the overall number of elements keeping the mesh dense enough in the most sensitive regions and less dense in other ones. It has been found that the essential feature of a good mesh (for the discussed structures) is large number of elements within the necks with relatively coarse mesh inside inclusions. The strain gradient is the quantity conditioning the mesh density – coarse mesh is enough to reflect only a small strain gradient.

Remark: In the case of empty inclusions ($E_{incl} = 0$), which were calculated as well, there is only the continuum of matrix. Therefore the constrained nodes were only those of shown in Fig. 1 which belong to the matrix. This was due to the lack of material in the corners of box.

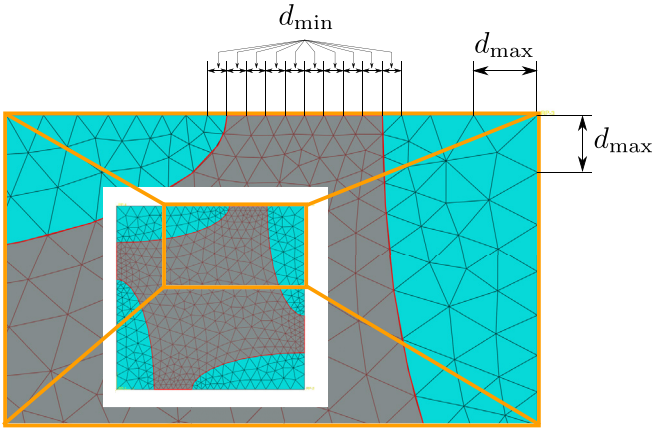

Fig. 2. Nonuniform exemplary mesh. Each edge was assigned a bias seed in order to obtain possibly dense mesh in the narrowest (neck) regions. In this case $L_{gap}/d_{min} = 8$ was chosen in order to make he figure readable. In the simulations this ratio was 100. Fig. 3 shows that the convergence tests were performed up to the value $d_{min} = 10^{-4}$.

The mesh heterogeneity is achieved by using a proper distribution of the nodes along the elliptic arcs, see Fig. 2. To generate a desired non-uniform mesh, both external (boundaries) and internal (interface) edges have been divided into segments of varying length. The sizes of the segments change as in the geometrical sequence. Parameters $d_{\min}$ and $d_{\max}$ together with the number of segments define the sequence:

$d_{\min}$ – the shortest segment,

$d_{\max}$ – the longest segment

on the considered segment. Thus, the ratio of $L_{gap}/d_{\min}$ defines the number of "layers" along the thinnest matrix regions (between the closest inclusions). Each of 4 edges of length L_{gap} (this might be considered the bottleneck thickness) within RUC quarter is divided in the same way.

The proper choice of values for parameters $d_{\min}$ and $d_{\max}$ ensures a good convergence within satisfying computational time and resources consumption. In Fig. 3 the convergence of Poisson's ratio as function of $d_{\min}$ for the constant value $d_{\max} = 0.01$ is presented. It can be seen there that when $d_{\min} \approx 0.0002$ the accuracy for the computed ν_{eff} is better than 0.005 and for $E_{\text{eff}}/E_{\text{matr}}$ is better than 0.0016 when $d_{\max} \approx 0.0002$.

In the Appendix A the results obtained for nonuniform meshes (i.e. with $d_{\max} > d_{\min}$) are compared with "uniform" ones (i.e. with $d_{\max} = d_{\min}$). It can be seen that the agreement between both the approaches in the limit of infinitely dense mesh is perfect. This leads to the following set of parameters used for the further simulations: $d_{\min} = 2 \cdot 10^{-4}$ and $d_{\max} = 10^{-2}$. This choice implies that for $L_{gap} = 0.02$ the matrix neck is divided into ca. 100 layers of triangular elements ($L_{gap}/d_{\min} = 100$). This number might seem to be overestimated (In fact, as it can be seen in the Appendix A, for $E_{\text{incl}}/E_{\text{matr}} \geq 1$ much smaller divisions give the required accuracy.). However, for extremely small values of L_{gap}, low values of inclusion Poisson's ratio, ν_{incl}, and low values of the ratio $E_{\text{incl}}/E_{\text{matr}} < 10^{-2}$, such a choice is necessary to provide accurate solutions, see Fig. 3. In particular, for $E_{\text{incl}} = 10^{-4}$ the convergence curve differs from the others. This behaviour can be considered as a warning pointing out that low density meshes should be avoided. The nonlinearity of the dependence shown there seems to have its origin in the fact that in

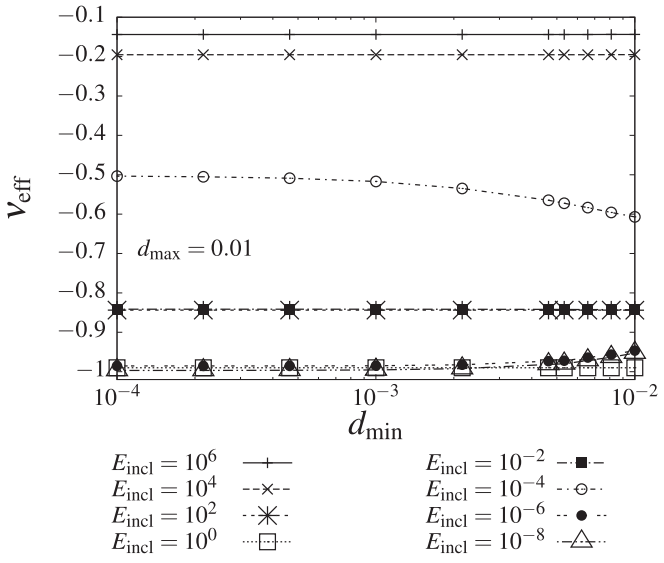

Fig. 3. Convergence of Poisson's ratio as a function of $d_{\min}$ at fixed $d_{\max} = 0.01$. Here $\nu_{\text{matr}} = \nu_{\text{incl}} = -0.99$, $E_{\text{matr}} = 1$. The geometric parameters are: $a = 0.09$, $b = 0.89$. The convergence displays various characteristics depending on the value of E_{incl}.

the vicinity of $E_{\text{incl}} = 10^{-4}$ the derivative $\partial\nu_{\text{eff}}/\partial E_{\text{incl}}$ takes high values. As such a behaviour could not be excluded *a priori* for other $E_{\text{incl}}/E_{\text{matr}}$ values, the nonuniform meshes with $d_{\min} \approx 0.0002$ and $d_{\max} \approx 0.01$ were used.

The finite element method was employed in order to solve the described boundary value problem. More precisely, ABAQUS/Standard 6.10 [48] was used utilizing CPS3 elements. These elements represent the plane stress formulation, which, in contrast to the plane strain theory, admits ν to take values from the range $\langle -1, 1\rangle$. The latter is characteristic for the pure 2D elasticity. (In particular, the expression for Lamé coefficient in plane stress $\lambda = E\ \nu/[(1-\nu)(1+\nu)]$ [49] determining the limits of ν is the same for plane stress elasticity and pure 2D elasticity.). The large number of systems with varying geometries and material parameters was possible to generate and solve thanks to the advantages of Python scripting interface (part of ABAQUS/Cae). The results presented in Fig. 4a–c (as well as in B1–B2 in the Appendix B) were obtained with the number of runs equal to 9900.

4. Results and discussion

$E_{\text{incl}}/E_{\text{matr}}$ runs over fourteen orders of magnitude from 10^{-8} to 10^{6} using 43 steps in the logarithmic scale. (Two more cases corresponded to voids and perfectly rigid inclusions, respectively.) In this section the attention is focused on the two extreme geometries $\{a = 0.09, b = 0.89\}$ (strongly elliptic) $\{a = 0.49, b = 0.49\}$ (circular) as well as the intermediate one $\{a = 0.29, b = 0.69\}$ which are shown in Fig. 4a, c b, respectively. More results for elliptic cases can be seen in the Appendix section – Figs. B1 and B2. Each figure consists of four plots in the vertical arrangement presenting various values of ν_{matr} from −0.99 to 0.49. In turn, each plot consists of two series of curves corresponding to various values of ν_{incl}. The first series of blue lines stands for the effective Poisson's ratio, while the red series describes the effective Young's modulus. (Colours are available in the online version.)

As mentioned earlier, the ratio $E_{\text{incl}}/E_{\text{matr}}$ is of great importance. One can roughly distinguish three cases of the ratio value:

1. the void limit inclusion, $E_{\text{incl}} \to 0$,
2. the homogeneous material (in the sense of Young's modulus), i.e. $E_{\text{incl}} = E_{\text{matr}}$,
3. the limit of perfectly rigid inclusion $E_{\text{incl}} \to \infty$.

Between the above cases there are two transition regions, further referred to as (1–2) and (2–3). These five cases are discussed below.

Case 1 When $E_{\text{incl}} \to 0$ the inclusions are extremely soft, approximating a model in which the material of inclusions is removed. The Poisson's ratio in this limit is very close to −1 and does not depend on the material parameters. This description is true as long as $a/b \neq 1$ when the rotating rigid units mechanism [11,17] is present. In Fig. B2c one may notice that the value of effective Poisson's ratio in the void limit is slightly above −1. This is due to the finite thickness of the hinge realised by the neck of dimension L_{gap}. In the special case $a/b = 1$, see Fig. 4c the auxeticity originating from the rotating rigid units mechanism or structural auxeticity is no more present. In Fig. 5a the results for void inclusions can be seen. In this simulations the material of inclusion was removed. The plot shows the dependence of ν as a function as the a/b ratio for various values of L_{gap}. The asymptotic analysis indicates that in the limit $L_{gap} \to 0$ the Poisson's ratio has a jump from −1 to a value close to 0 when $a/b \to 1$. These results remain in agreement with those presented in [17].

Case 2 $E_{\text{incl}} = E_{\text{matr}}$ represents a composite being uniform in the term of Young's modulus. In addition, if $\nu_{\text{incl}} = \nu_{\text{matr}}$, the material is completely homogeneous. In this case the effective Poisson's ratio

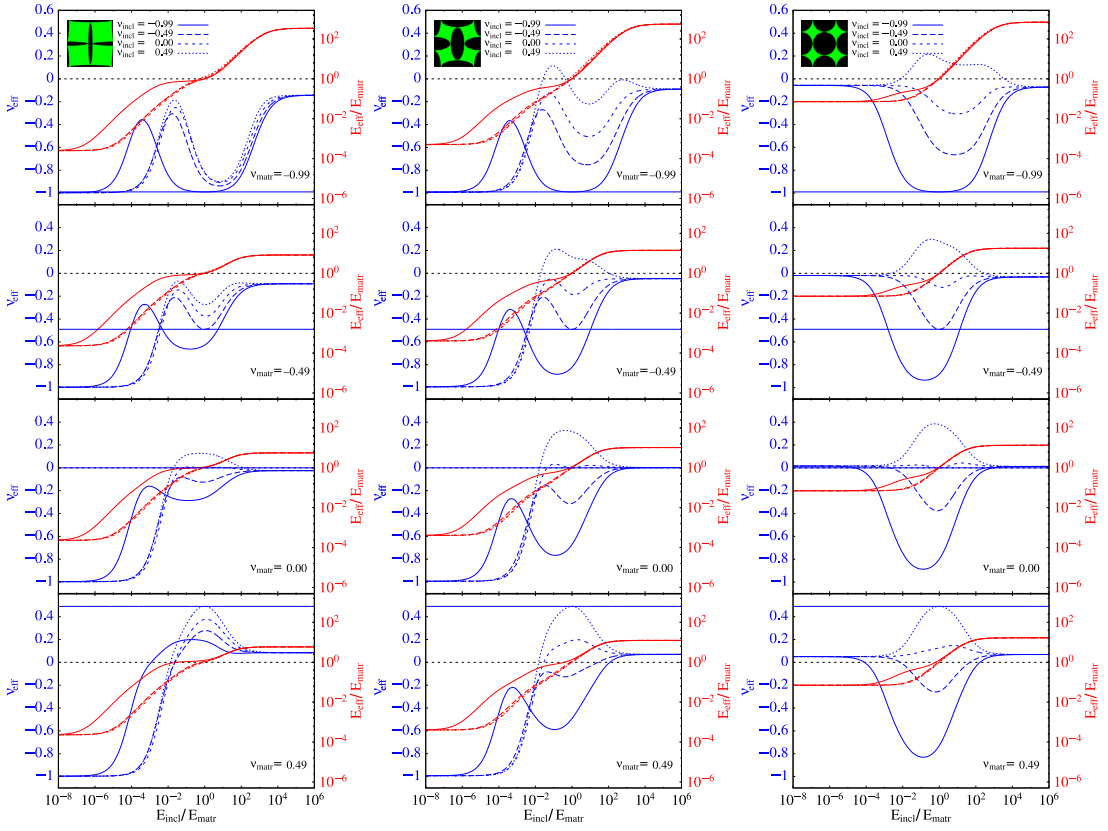

Fig. 4. Effective Poisson's ratio, ν_{eff}, and effective Young's modulus, E_{eff}/E_{matr}, as functions of E_{incl}/E_{matr} for various ν_{incl} and ν_{matr} (see plot legends) for selected geometries (defined by the parameters a and b). The monotonously increasing curves, roughly grouped in bands, represent the values of E_{eff}. Any other, i.e. non-monotonously changing curves, represent the effective PR.

as well as the Young's modulus are of course equal to the material ones. In Fig. 4 (and Figs. B1 and B2 in the Appendix B) the blue horizontal lines denote effective PR, ν_{eff}, for the case $E_{incl}/E_{matr} = 1$ with $\nu_{incl} = \nu_{matr}$. The curve representing ν_{eff} for certain value of ν_{incl} equal to ν_{matr} is tangent to the blue horizontal line for $E_{incl}/E_{matr} = 1$. The effective Young's modulus represented by the red lines series normalized to E_{matr} is then close to the value 1 which is obvious.

In the discussed range of values $E_{matr} \approx E_{incl}$ with $\nu_{incl} < \nu_{matr}$ the closer the ratio a/b to 1 the lower the effective Poisson's ratio of the composite is. This is because as $a/b \to 1$ for the fixed L_{gap}, the volume fraction of "less auxetic" matrix in RUC decreases.

Of special interest is the **Case 3**. Here the limit of perfectly rigid inclusions is reached. Fig. 4a for $\nu_{matr} = 0$ (third plot as counted from the top) reveals an interesting property. The Poisson's ratio (most right side of the plot) is negative (roughly equal to -0.024), while both constituents (inclusions and matrix) have non-negative Poisson's ratio. This auxeticity, similarly as in the Case 1, has a structural origin and it is neither induced by Poisson's ratios of inclusions nor matrix. For very hard inclusions ($E_{matr} \to \infty$), like in the case of very soft ($E_{matr} \to 0$), the value ν_{incl} does not have any influence on the effective properties. In the rigid limit the inclusions simply do not deform. As shown in the Appendix B (Figs. B1a and B1b) the effect of negative PR, induced by rigid inclusions, vanishes as the ratio a/b approaches the value 1. This dependence is clearly seen in Fig. 5b. For certain critical value of a/b ratio the composite built of non-auxetic materials with rigid inclusions becomes auxetic. What is interesting, this phenomenon does not vanish for the relatively large values of L_{gap}. In turn, Fig. 6 presents the dependence of ν_{eff} as a function of L_{gap} for various values of a/b ratio. The lowest value of ν_{eff} is achieved at $L_{gap} \approx 0.2$ and is close to -0.07.

Another interesting aspect of the investigated composites is the behaviour of effective Poisson's ratio as a function of the matrix Poisson's ratio (ν_{matr}) in the limit of rigid inclusions, i.e. $E_{incl} \to \infty$. This dependence is shown in Fig. 7. A constant value of $L_{gap} = 0.02$ is preserved for all plotted (a, b) pairs. In the inset plot the effective Poisson's ratio is plotted against $\log(a/b)$ for the fixed $\nu_{matr} = 0$. Between the configurations ($a = 0.24$, $b = 0.74$) and ($a = 0.29$, $b = 0.69$), corresponding the $a/b \approx 0.32$ and $a/b \approx 0.42$, respectively, the change of ν_{eff} sign is observed. The auxeticity of the whole composite in the case of $\nu_{matr} = 0$ is present as along as the a/b ratio does not exceed the value of ca. $a/b = 0.365$ (see the inset in Fig. 7). This ratio corresponds to the inclusion volume fraction roughly equal to 0.591. Fig. 7 convinces that is it possible to obtain a negative effective Poisson's ratio for $\nu_{matr} > 0$. What is even more important, the resulting structure is continuous, i.e. no holes or cuts are present, and the inclusions are harder than the matrix.

The transitional range of E_{incl} values between Case 1 and Case 2 denoted as (**1**–**2**) is the region where the mechanism of rotating rigid unit is systematically suppressed. This means that the structural auxeticity gradually vanishes when the value of E_{incl}/E_{matr} increases from 10^{-8} to 1. The harder the inclusions (in the sense of Young's modulus) the more deformation energy in consumed by them, what in turn interferes with the rotation of square-like formerly almost rigid units (as compared to void inclusions). Except the case of $a/b = 1$ (for $\nu_{incl} \leq 0.0$) the increase of effective Poisson's ratio is observed. The effective Young's modulus also increases in this region, in particular, for the most auxetic inclusions the effective Young's modulus, E_{eff}, is large as compared to the other ν_{incl}. This effect (especially noticeable in Fig. 4a) is important because many auxetics are rather soft materials. An important

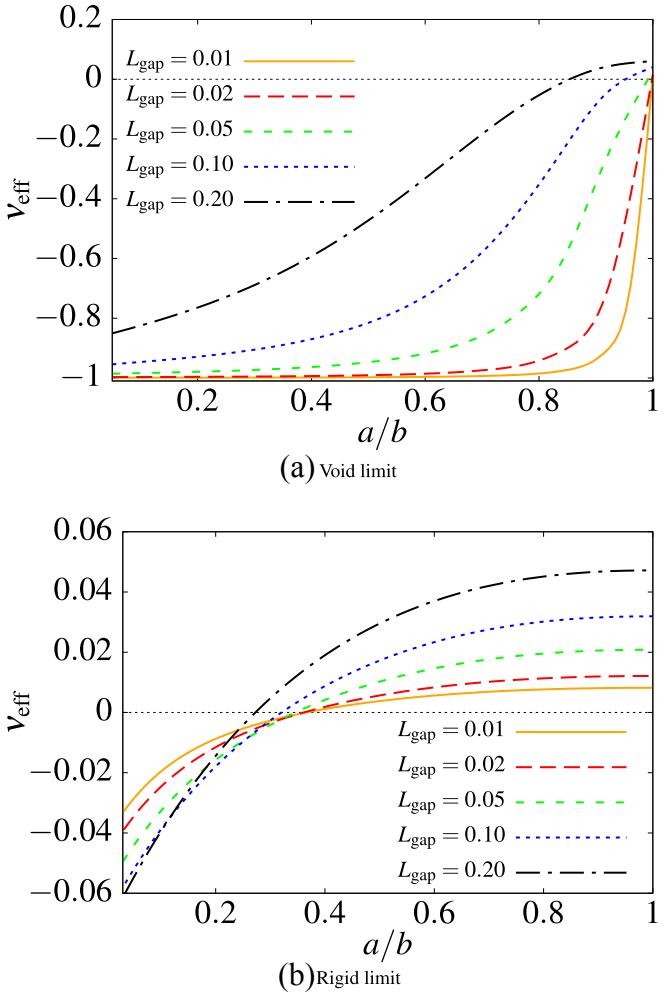

Fig. 5. The dependence of Poisson's ratio as a function of a/b for various values of L_{gap}. Here both ν_{matr} and ν_{incl} are equal 0.

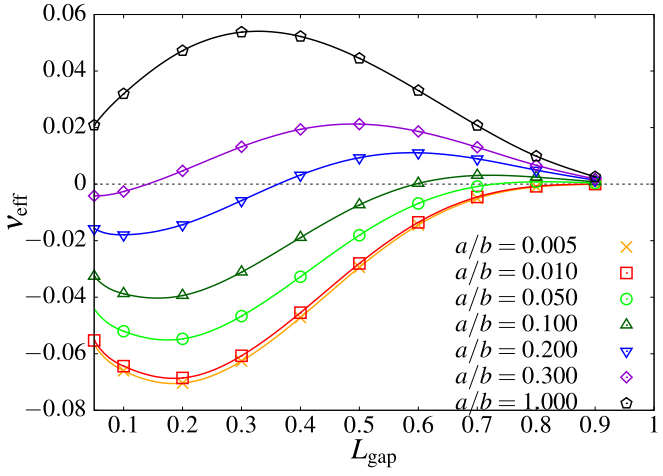

Fig. 6. The dependence of Poisson's ratio as a function of L_{gap} for various values of a/b within the rigid inclusion limit. Here as in Fig. 5, both ν_{matr} and ν_{incl} are equal 0.

observation is that very soft ($E_{incl} \to 0$) and very auxetic ($\nu_{incl} \to -1$) inclusions give the contribution to the overall composite hardness (E_{eff}) remaining the effective Poisson's ratio unchanged within a small window of E_{incl}/E_{matr} values. Further increase of E_{incl}/E_{matr} causes an increase of both E_{eff} and ν_{eff}.

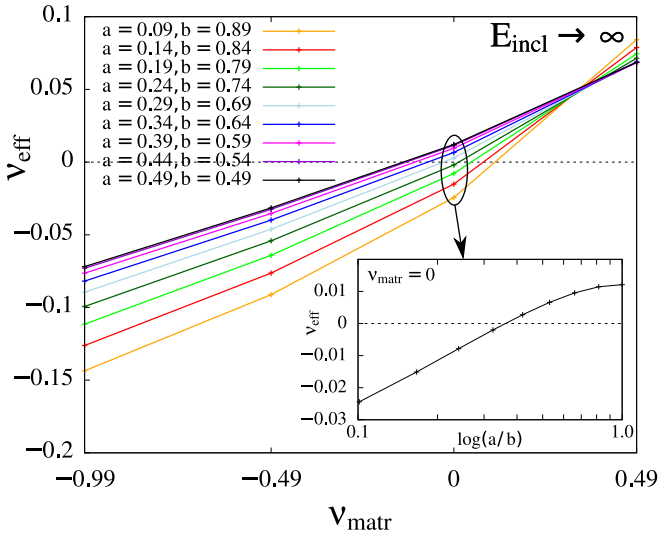

Fig. 7. The dependence of effective Poisson's ratio as a function of the matrix Poisson's ratio in the limit of infinitely hard inclusions ($E_{incl} \to \infty$). The value of ν_{incl} in this limit has no impact on the effective properties since the inclusions do not deform. The inset figure helps in estimating of the a/b ratio, for which ν_{eff} changes sign. Curves in the black and white printing can be easily identified: at the point $\nu_{matr} = -0.99$ the lines are reversely ordered with respect to the legend.

A surprising effect is that, for strongly auxetic inclusions, the effective Poisson's ratio which initially increases with increasing E_{incl}/E_{matr} then *decreases* when E_{incl}/E_{matr} approaches unity. It is worth to stress that, as seen in Fig. 8, the maximum of the effective Poisson's ratio moves to lower values of E_{incl}/E_{matr} with increasing auxeticity of the matrix and inclusions. One should add that more auxetic inclusions imply higher effective Young's modulus in the vicinity of the mentioned maximum of the Poisson's ratio.

The transitional region between Case 2 and Case 3, denoted as (**2**–**3**), accords with the values of E_{incl}/E_{matr} from 1 up to the plateau attainment. In this region the inclusions are harder than the matrix, i.e. $E_{incl} > E_{matr}$. The effective Young's modulus continues its monotonous increase to reach a plateau, which value depends on the geometry and ν_{matr} only. The effective Poisson's ratio changes its value depending on the geometry (a/b ratio) and both values ν_{incl} and ν_{matr}. The behaviour of effective Poisson's ratio i (2–3) is in general non-monotonous.

An analysis of large deformations, leading to nonlinearity has been also performed in the limit of void inclusions, $E_{incl} \to 0$, i.e. with

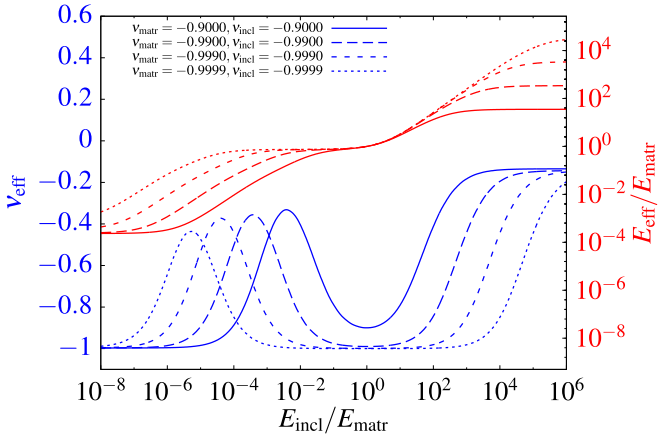

Fig. 8. Effective Poisson's ratio, ν_{eff}, (blue colour) and effective Young's modulus, E_{eff}/E_{matr}, (red colour) as functions of E_{incl}/E_{matr} for strongly auxetic matrices and inclusions. (For interpretation of the references to colour in this figure legend, the reader is referred to the web version of this article.)

removed material of inclusions. It should be stressed, that the linear (Hookean) material is considered, and the only source of the nonlinearity is the third term in the Green strain tensor: $\varepsilon_{ij} = 1/2(\partial U_i/\partial x_j + \partial U_j/\partial x_i + \partial U_k/\partial x_i \partial U_k/\partial x_j)$. The results for effective ν and E are presented, respectively, in Fig. 9a and b. As one can see there, Fig. 9a, the effective Poisson's ratio increases with increasing strain, however, as $a/b \to 1$ for high strains, a slight decrease of the effective Poisson's ratio is observed. For the effective Young's modulus, Fig. 9b, the behaviour is similar. The decrease of the effective Young's modulus for more isotropic inclusions ($a/b \approx 1$) being even stronger is still moderate, however. The lower the a/b ratio value the system is more resistive to changes or, in other words, the system "keeps" its initial effective properties "longer" during deformation. This behaviour may be explained on the basis of the theory of rotating rigid objects [12]. As the a/b ratio is closer to 0 the more rotation of rigid units is possible. This means that the lower a/b then the system deforms through rotation for larger values of the applied strain.

As long as the deformation manifests through rotation, both ν_{eff} and E_{eff} remain low. As the deformation continues, the rotation is gradually suppressed in favour of the neck (hinges) stretching, which causes both ν_{eff} and E_{eff} increase. In Fig. 9a a rapid increase of the effective Poisson's ratio as a function of a/b ratio in the limit of infinitesimally small strain is observed (the jump from pink line through violet to black). In the limit of $L_{\text{gap}} \to 0$ this change is described with the Heaviside's step function. For $a/b = 1$ no rotation occurs, so no auxeticity is observed.

In most of the simulations presented above the neck thickness was equal to $L_{\text{gap}} = 0.02$. For other values of L_{gap} the qualitative dependence of ν_{eff} and $E_{\text{eff}}/E_{\text{matr}}$ on $E_{\text{incl}}/E_{\text{matr}}$ was qualitatively similar.

The results obtained with ABAQUS/Standard were verified by simulations performed in COMSOL Multiphysics. The agreement was excellent.

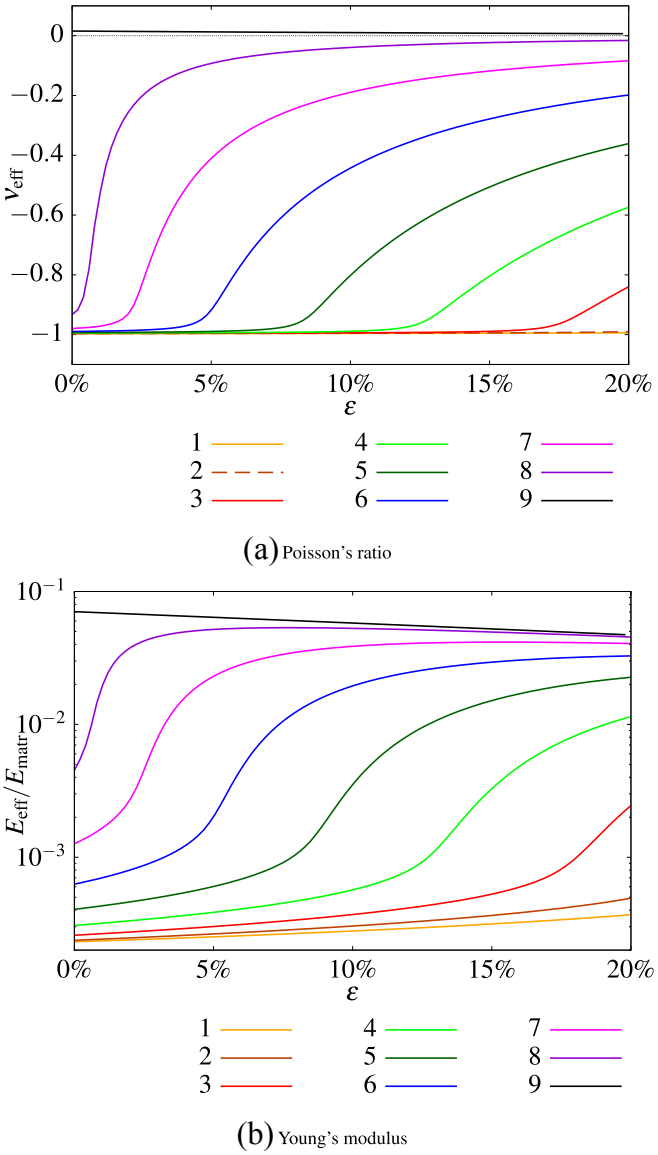

Fig. 9. Effective Poisson's ratio, ν_{eff}, and effective Young's modulus, $E_{\text{eff}}/E_{\text{matr}}$ as functions of nominal strain for $\nu_{\text{matr}} = 0$ and "void" inclusions (the material of inclusions is entirely removed) under nonlinear load – large displacement. The numbers in the legend correspond to the following geometry parameter pairs: 1) $a = 0.09, 0.89$, 2) $a = 0.14, 0.84$, 3) $a = 0.19, 0.79$, 4) a = 0.24, 0.74, 5) $a = 0.29, 0.69$, 6) $a = 0.34, 0.64$, 7) $a = 0.39, 0.59$, 8) $a = 0.44, 0.54$, 9) $a = 0.49, 0.49$.

5. Conclusion

Finite Element studies of the effective Poisson's ratio and Young's modulus corresponding to stresses acting in the x-axis direction were done for composites with elliptic inclusions. (The general case of the stress acting in *any* direction will be a subject of the future work.) Various parameters of both geometric and material type were considered. It has been found that for very soft inclusions the dominating mechanism is that of rotating rigid units what leads to almost perfect auxeticity, i.e. Poisson's ratios close to -1. In turn, for the opposite limit, i.e. for rigid inclusions, the auxeticity has been observed as well. Despite it was weaker than in the case of void 'inclusions', the auxeticity from rigid inclusions can be of interest from the point of view of potential applications. This is because its effective Young's modulus is high. So, in both limits of E_{incl} the auxeticity can be achieved for the conventional (non-auxetic) materials! What concerns the effective Young's modulus, the present studies showed that very soft inclusions ($E_{\text{incl}} \to 0$) with extremely low Poisson's ratio ($\nu_{\text{incl}} \to -1$) can essentially increase the effective Young's modulus. In a range of small $E_{\text{incl}}/E_{\text{matr}}$ ratios, this increase is accompanied by very low values of ν_{eff}. When the Young's modulus of inclusions grows, the price for increasing E_{eff} is the reduction of effective auxeticity.

Acknowledgements

This work was supported by the (Polish) National Centre for Science under the grant NCN 2012/05/N/ST5/01476.

Appendices

Appendix A

In Fig. A1 the convergence for increasing mesh quality, described with a parameter $L_{\text{gap}}/d_{\text{min}}$ changing from 5 to 800, is presented. Clearly, the non-uniform mesh generated for parameter $L_{\text{gap}}/d_{\text{min}} = 100$ is satisfying for the selected geometrical and material quantities. Moreover, in Figs. A2 and A3 the asymptotic behaviour for Poisson's ratio and Young's modulus is presented, respectively. Red circles in the plots show the effective elastic constants obtained for uniform meshes as a function of $1/n_l$, i.e. the reciprocal of number of layers along the neck ($n_l \equiv L_{\text{gap}}/d_{\text{min}}$). Each blue square in the plot represents the limit of $d_{\text{min}} \to 0$ for fixed d_{max}. Finally there are two limits presented by cross symbols: $\times$ – uniform and – non-uniform mesh, where the limit for non-uniform meshes (the 2nd one) is taken for $d_{\text{max}} \to 0$.

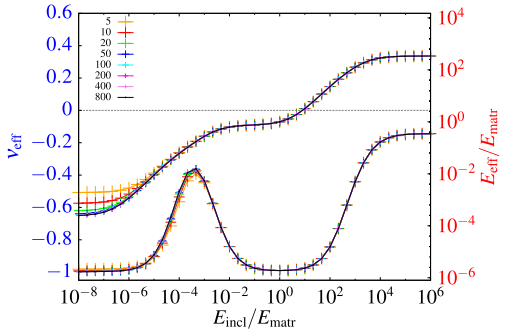

Fig. A1. Convergence of ν_{eff} and $E_{\text{eff}}/E_{\text{matr}}$ as obtained within non-uniform meshing for $a = 0.09$, $b = 0.89$, $\nu_{\text{incl}} = \nu_{\text{matr}} = -0.99$ and increasing mesh density. The upper, monotonic curves refer to the right (Young's modulus, red) axis, while the non-monotonic curves refer to the left (Poisson's ratio, blue) axis. The numbers in the legend stand for the $L_{\text{gap}}/d_{\text{min}}$ ratio. (For interpretation of the references to colour in this figure legend, the reader is referred to the web version of this article.)

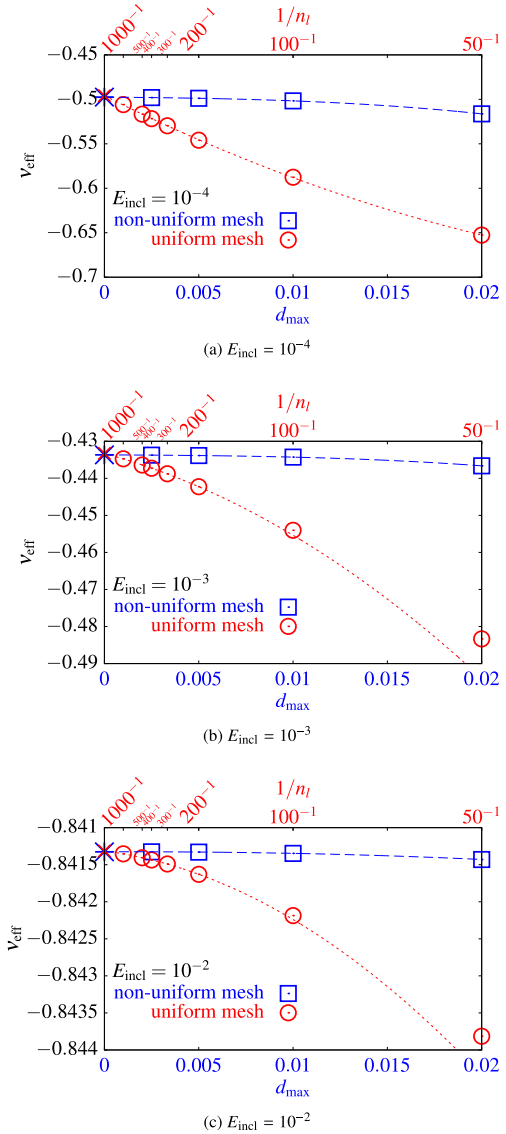

Fig. A2. Effective Poisson's ratio, ν_{eff}, as a function of d_{max} for uniform (red) and non-uniform (blue) meshing rules taken for three different values of E_{incl}, here $a = 0.09$, $b = 0.89$, while $\nu_{\text{incl}} = \nu_{\text{matr}} = -0.99$. The cross symbols (red $\times$ and blue) denote the values of limits of infinitely dense meshes for uniform and non-uniform rules, respectively. The fits were performed using low order polynomials. Red lines were fitted intentionally skipping two "worst" points. (For interpretation of the references to colour in this figure legend, the reader is referred to the web version of this article.)

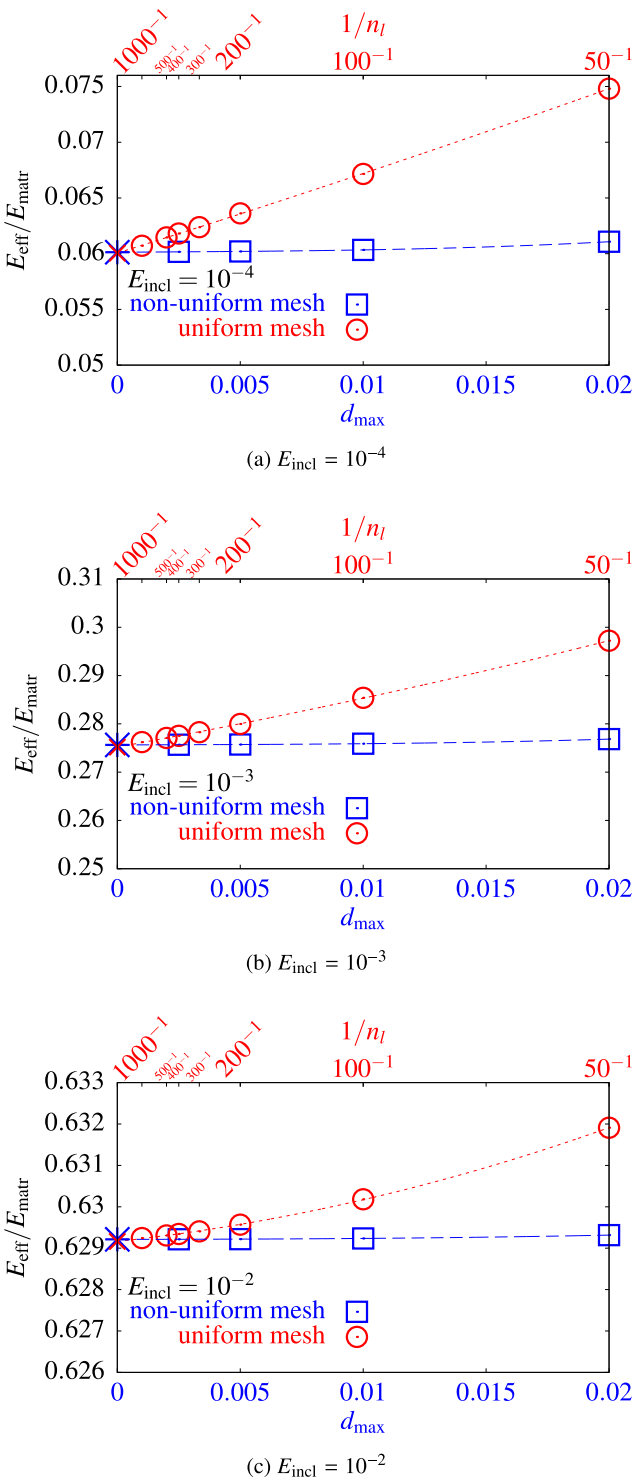

Fig. A3. Effective Young's modulus, $E_{\text{eff}}/E_{\text{matr}}$, as a function of d_{max}. The symbols as in Fig. A2.

Appendix B

Figs. B1 and B2 show the effective Poisson's ratio and Young's modulus dependence on material properties of the matrix and inclusions for selected intermediate, with respect to those presented in Fig. 4, geometries of the composite.

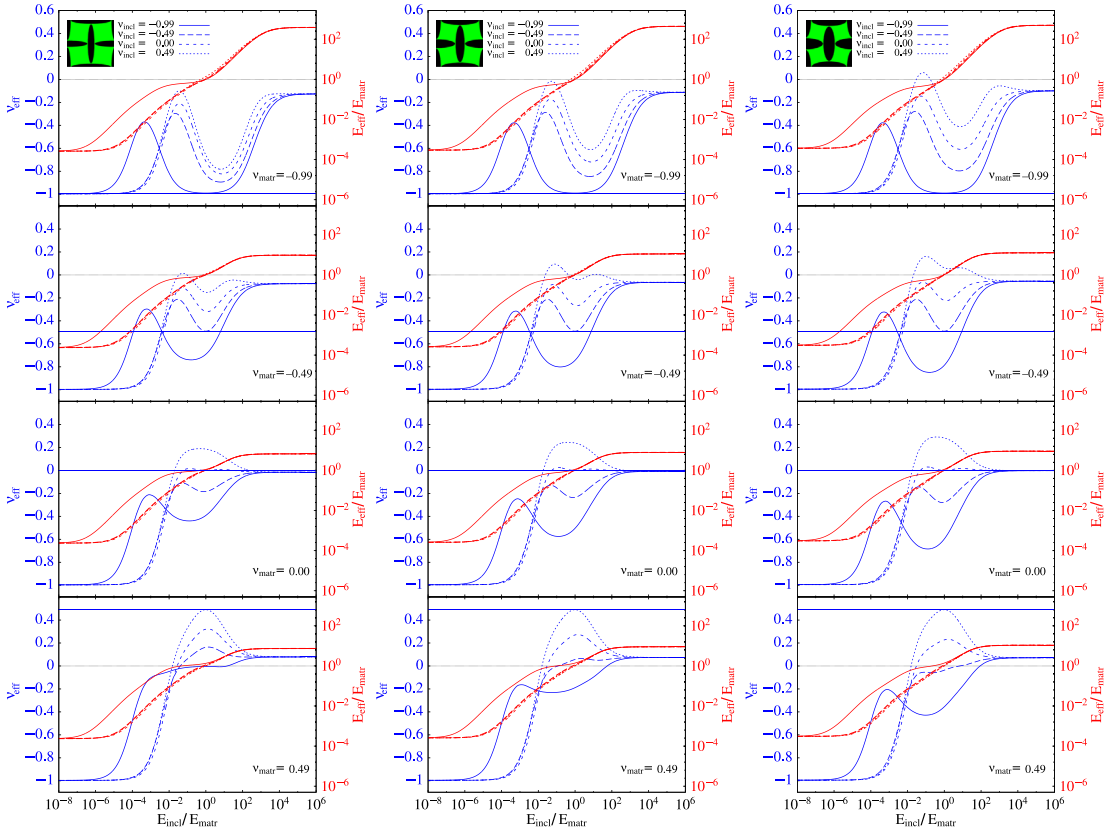

(a) $a = 0.14,\ b = 0.84$ (b) $a = 0.19,\ b = 0.79$ (c) $a = 0.24,\ b = 0.74$

Fig. B1. ν_{eff} and $E_{\text{eff}}/E_{\text{matr}}$ as functions of $E_{\text{incl}}/E_{\text{matr}}$ for various ν_{incl} and ν_{matr} (see plot legends) for selected geometries (defined by the parameters a and b). In the black and white printing the distinction between curves representing effective PR and Young's modulus is the same as it was indicated in the caption to Fig. 4.

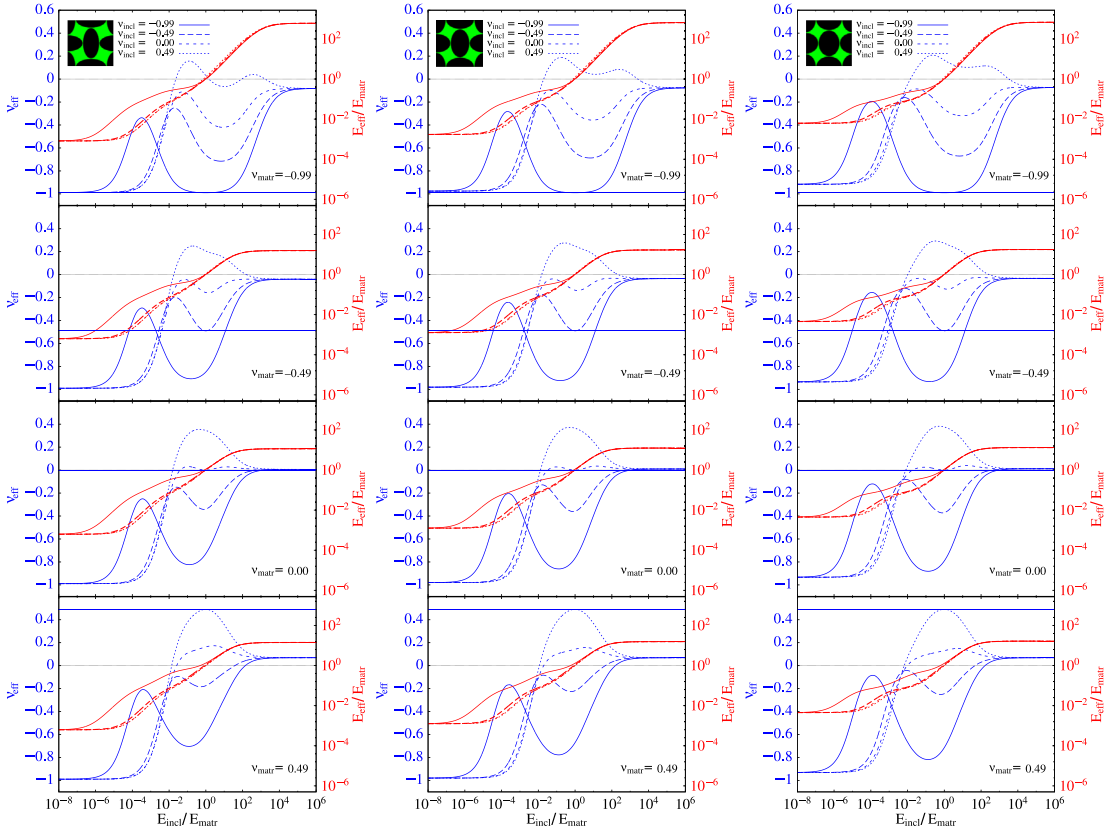

(a) $a = 0.34,\ b = 0.64$ (b) $a = 0.39,\ b = 0.59$ (c) $a = 0.44,\ b = 0.54$

Fig. B2. ν_{eff} and $E_{\text{eff}}/E_{\text{matr}}$ as functions of $E_{\text{incl}}/E_{\text{matr}}$ for various ν_{incl} and ν_{matr} (see plot legends) for selected geometries (defined by the parameters a and b). In the black and white printing the distinction between curves representing effective PR and Young's modulus is the same as it was indicated in the caption to Fig. 4.

References

[1] Lakes RS. Foam structures with a negative Poisson's ratio. Science 1987;235(4792):1038–40. http://dx.doi.org/10.1126/science.235.4792.1038.

[2] Lakes RS. Response: negative Poisson's ratio materials. Science 1987;238(4826):551. http://dx.doi.org/10.1126/science.238.4826.551-a.

[3] Evans KE. Auxetic polymers: a new range of materials. Endeavour 1991;15(4):170–4.

[4] Almgren RF. An isotropic three-dimensional structure with Poisson's ratio =−1. J Elast 1985;15(4):427–30.

[5] Wojciechowski KW. Constant thermodynamic tension Monte Carlo studies of elastic properties of a two-dimensional system of hard cyclic hexamers. Mol Phys 1987;61(5):1247–58.

[6] Alderson A, Alderson KL, Attard D, Evans KE, Gatt R, Grima JN, et al. Elastic constants of 3-, 4- and 6-connected chiral and anti-chiral honeycombs subject to uniaxial in-plane loading. Compos Sci Technol 2010;70(7):1042–8.

[7] Bettini P, Airoldi A, Sala G, Landro LD, Ruzzene M, Spadoni A. Composite chiral structures for morphing airfoils: numerical analyses and development of a manufacturing process. Compos Part B Eng 2010;41(2):133–47. http://dx.doi.org/10.1016/j.compositesb.2009.10.005.

[8] Gaspar N, Smith C, Alderson A, Grima JN, Evans KE. A generalised three-dimensional tethered-nodule model for auxetic materials. J Mater Sci 2010;46(2):372–84.

[9] He G, Tan Q, Jiang G, Li Q. A novel mechanism for auxetic behavior in entangled materials with a spiral wire structure. Smart Mater Struct 2014;23(9). 095011.

[10] Mizzi L, Attard D, Gatt R, Pozniak AA, Wojciechowski KW, Grima JN. Influence of translational disorder on the mechanical properties of hexachiral honeycomb systems. Compos Part B Eng 2015;80:84–91.

[11] Grima JN, Evans KE. Auxetic behavior from rotating squares. J Mater Sci Lett 2000;19(17):1563–5.

[12] Grima JN, Alderson A, Evans KE. Auxetic behaviour from rotating rigid units. Phys Status Solidi B 2005;242(3):561–75.

[13] Grima JN, Zammit V, Gatt R, Alderson A, Evans KE. Auxetic behaviour from rotating semi-rigid units. Phys Status Solidi B 2007;244(3):866–82.

[14] Attard D, Grima JN. A three-dimensional rotating rigid units network exhibiting negative Poisson's ratios. Phys Status Solidi B 2012;249(7):1330–8.

[15] Slann A, White W, Scarpa F, Boba K, Farrow I. Cellular plates with auxetic rectangular perforations. Phys Status Solidi B 2015;252:1533–9.

[16] Grima JN, Jackson R, Alderson A, Evans KE. Do zeolites have negative Poisson's ratios? Adv Mater 2000;12(24):1912–8.

[17] Taylor M, Francesconi L, Gerendás M, Shanian A, Carson C, Bertoldi K. Low porosity metallic periodic structures with negative Poisson's ratio. Adv Mater (Deerfield Beach, FL) 2014;26(15):2365–70.

[18] Wu G, Cho Y, Choi I-S, Ge D, Li J, Nam Han H, et al. Directing the deformation paths of soft metamaterials with prescribed asymmetric units. Adv Mater 2015;27(17):2747–52.

[19] Shan S, Kang SH, Zhao Z, Fang L, Bertoldi K. Design of planar isotropic negative Poisson's ratio structures, Extreme Mech Lett. 10.1016/j.eml.2015.05.002.

[20] Bertoldi K, Boyce MC, Deschanel S, Prange SM, Mullin T. Mechanics of deformation-triggered pattern transformations and superelastic behavior in periodic elastomeric structures. J Mech Phys Solids 2008;56:2642–68. http://dx.doi.org/10.1016/j.jmps.2008.03.006.

[21] Grima JN, Gatt R. Perforated sheets exhibiting negative Poisson's ratios. Adv Eng Mater 2010;12(6):460–4. http://dx.doi.org/10.1002/adem.201000005.

[22] Cho Y, Shin J-h, Costa A, Kim TA, Kunin V, Li J, et al. Engineering the shape and structure of materials by fractal cut. Proc Natl Acad Sci USA 2014;111(49):17390–5. http://dx.doi.org/10.1073/pnas.1417276111.

[23] Gatt R, Mizzi L, Azzopardi JI, Azzopardi KM, Attard D, Casha A, et al. Hierarchical auxetic mechanical metamaterials. Sci Rep 2015;5:8395. http://dx.doi.org/10.1038/srep08395.

[24] Mizzi L, Azzopardi KM, Attard D, Grima JN, Gatt R. Auxetic metamaterials exhibiting giant negative Poisson's ratios. Phys Status Solidi (RRL) Rapid Res Lett 2015;9. http://dx.doi.org/10.1002/pssr.201510178.

[25] Bertoldi K, Reis PM, Willshaw S, Mullin T. Negative Poisson's ratio behavior induced by an elastic instability. Adv Mater (Deerfield Beach, FL) 2010;22(3):361–6.

[26] Wei G, Edwards SF. Poisson ratio in composites of auxetics. Phys Rev E 1998;58(5):6173–81.

[27] Wei G, Edwards SF. Auxeticity windows for composites. Phys A Stat Mech Appl 1998;258(1–2):5–10.

[28] Wei G, Edwards SF. Effective elastic properties of composites of ellipsoids (I). Nearly spherical inclusions. Phys A Stat Theor Phys 1999;264(3–4):388–403.

[29] Wei G, Edwards SF. Effective elastic properties of composites of ellipsoids (II). Nearly disk- and needle-like inclusions. Phys A Stat Theor Phys 1999;264(3–4):404–23.

[30] Assidi M, Ganghoffer JF. Composites with auxetic inclusions showing both an auxetic behavior and enhancement of their mechanical properties. Compos Struct 2012;94(8):2373–82.

[31] Strek T, Jopek H. Effective mechanical properties of concentric cylindrical composites with auxetic phase. Phys Status Solidi B 2012;249(7):1359–65.

[32] Strek T, Jopek H, Maruszewski BT, Nienartowicz M. Computational analysis of sandwich-structured composites with an auxetic phase. Phys Status Solidi B 2014;251(2):354–66.

[33] Jopek H, Strek T. Thermal and structural dependence of auxetic properties of composite materials. Phys Status Solidi B 2015;252(7):1551–8. http://dx.doi.org/10.1002/pssb.201552192.

[34] Strek T, Jopek H, Nienartowicz M. Dynamic response of sandwich panels with auxetic cores. Phys Status Solidi B 2015;252(7):1540–50. http://dx.doi.org/10.1002/pssb.201552024.

[35] Hou Y, Neville R, Scarpa F, Remillat C, Gu B, Ruzzene M. Graded conventional-auxetic Kirigami sandwich structures: flatwise compression and edgewise loading. Compos Part B 2014;59:33–42.

[36] Christensen RM. Effective properties for single size, rigid spherical inclusions in an elastic matrix. Compos Part B Eng 2004;35:475–82.

[37] Banks-Sills L, Leiderman V, Fang D. On the effect of particle shape and orientation on elastic properties of metal matrix composites. Compos Part B Eng 1997;28B(4):465–81.

[38] Pozniak AA, Smardzewski J, Wojciechowski KW. Computer simulations of auxetic foams in two dimensions. Smart Mater Struct 2013;22:084009. http://dx.doi.org/10.1088/0964-1726/22/8/084009.

[39] Banerjee S, Sankar BV. Mechanical properties of hybrid composites using finite element method based micromechanics. Compos Part B 2014;58:318–27.

[40] Wojciechowski KW. Simple models of anomalous mechanical properties. In: Joint conferences on advanced materials functional and nanostructured materials FNMA'11 intermolecular and magnetic interactions in matter IMIM'11 8th international workshop on auxetics and related systems AUXETICS'11, task, Gdansk; 2011.

[41] Sigmund O, Torquato S, Aksay IA. On the design of 1-3 piezocomposites using topology optimization. J Mater Res 1998;13(04):1038–48. http://dx.doi.org/10.1557/JMR.1998.0145.

[42] Pozniak AA, Wojciechowski KW. Poisson's ratio of rectangular anti-chiral structures with size dispersion of circular nodes. Phys Status Solidi B 2014;251(2):367–74.

[43] Landau LD, Lifshits EM. Theory of elasticity. London: Pergamon Press; 1986.

[44] Pindera M, Khatam H, Drago A, Bansal Y. Micromechanics of spatially uniform heterogeneous media: a critical review and emerging approaches. Compos Part B Eng 2009;40(5):349–78.

[45] Jafari A, Khatibi AA, Mashhadi MM. Comprehensive investigation on hierarchical multiscale homogenization using representative volume element for piezoelectric nanocomposites. Compos Part B Eng 2011;42(3):553–61.

[46] Xie X, Fan H. Effective modulus of heterogeneous materials in thin film configurations. Mater Sci Eng A 2010;527(21–22):5452–61. http://dx.doi.org/10.1016/j.msea.2010.05.028.

[47] Sadd MH. Elasticity: theory, applications, and numerics. Academic Press; 2009.

[48] Hibbit D, Karlsson B, Sorensen P. ABAQUS/standard analysis user's manual, ver. 6.10. 2010.

[49] Liu G-R, Quek SS. The finite element method: a practical course. Butterworth-Heinemann; 2003.